# LAMINAR-TURBULENT TRANSITION CORRELATION IN SUPERSONIC/HYPERSONIC FLOW

**George A. Simeonides*, Elias Kosmatopoulos****
**University of Patras, Dept. Mechanical and Aeronautical Engineering, Rio, Greece**
***also Hellenic Aerospace Industry, Tanagra, Schimatari, Greece**
****presently Imperial College, Dept. Civil Engineering**

**Keywords**: *transition, supersonic, flat plate, cone, bluntness*

## Abstract

*A correlation form, already established to represent a wide range of flat plate transition onset data at supersonic / hypersonic flow conditions, is implemented to correlate also high speed wind tunnel and in-flight transition over cones and complete vehicle configurations. The previously identified flat plate "strong bluntness" correlation is found to represent well the additional cone and vehicle (windward centreline) transition onset data in its range of application, but also provides an accurate transition "upper bound" throughout the complete data range. On the other hand, the flat plate "modest bluntness" correlation provides a transition "lower bound" in its range of application, where transition appears to be more sensitive to the disturbance environment.*

## List of symbols

| | |
|---|---|
| $b$ | leading edge or nose bluntness |
| $M$ | Mach number |
| $\mathrm{Re}_b$ | bluntness Reynolds number $= \frac{\rho u b}{\mu}$ |
| $\mathrm{Re}_{unit}$ | unit Reynolds number (per meter) |
| $\mathrm{Re}_{xtrans}$ | transition onset Reynolds number $= \frac{\rho u x_{tr}}{\mu}$ |
| $T$ | temperature |
| $u$ | stream-wise velocity |
| $x$ | stream-wise distance from the leading edge |

## Greek symbols

| | |
|---|---|
| $\alpha$ | angle of attack |
| $\mu$ | viscosity |
| $\rho$ | density |

## Subscripts

| | |
|---|---|
| *tr* | transition onset location |
| *w* | wall conditions |
| 0 | *total (stagnation) flow conditions* |

## 1 Introduction

Further to the successful correlation of a significant number of flat plate transition onset data in supersonic and hypersonic flow [1,2] that was presented at the previous ICAS Congress [3], the present paper examines the extension of the originally proposed flat plate correlation forms to transition over cones and complete vehicle configurations, also in the supersonic and hypersonic flow regime.

The following paragraphs present, first a brief review of the main findings of [3] in section 2, followed by the cone transition data analysis in section 3, and the examination of transition data over complete vehicle configurations (along the windward symmetry line) in section 4. It is noted that flight test data is included for a cone and the Space Shuttle Orbiter (STS flights 1 thru 5). The paper is concluded by a summary of all the data in the proposed correlation form and a brief discussion of the major findings.

## 2 Review of Flat Plate Results

The flat plate data of [4-14] has been presented in detail in [1-3], and correlated successfully in [3]; it covers a range in free-stream-based leading edge bluntness Reynolds number, $\mathrm{Re}_b$, between 20 and 100,000 and in free-stream-based transition onset Reynolds number, $\mathrm{Re}_{xtrans}$,

between 0.7 and 20 million, for Mach numbers between 2 and 8. Details of the flat plate data may be found in [1-3].

In the correlation presented in [3], the parameter ($Re_b/M^2$) serves as an independent variable and the parameter ($Mx_{trans}/b$) serves as the dependent variable (Fig. 1).

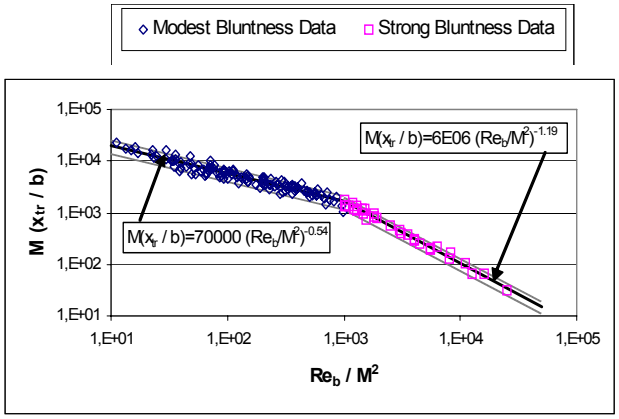


Fig. 1 Flat plate transition data correlation and mathematical representation [3]

In fact, two major distinct correlation regimes have been proposed in [3], depending on the bluntness of the leading edge of the flat plate, as follows:

- A modest bluntness regime (for $10 < Re_b/M^2 < 1000$), where data is represented (within +/- 30%) by:

$$Re_{xtrans} = 70000 M^{0.08} Re_b^{0.46} \qquad (1)$$

or closely approximated by:

$$Re_{xtrans} = 100000\, Re_b^{0.42} \qquad (2)$$

- A strong bluntness regime (for $Re_b/M^2 > 1000$), where data is represented (within +/- 25%) by:

$$Re_{xtrans} = 6 \cdot 10^6 M^{1.38} Re_b^{-0.19} \qquad (3)$$

At values of $Re_b/M^2$ lower than 10 (or 100), where leading edge bluntness effects become small, transition is viscous dominated and the data diverges from the modest and strong bluntness trends. Moreover, viscous dominated transition data has proven to be highly sensitive to the testing environment as illustrated in Fig. 2 by the behavior of the NASA quiet tunnel flat plate measurements [13].

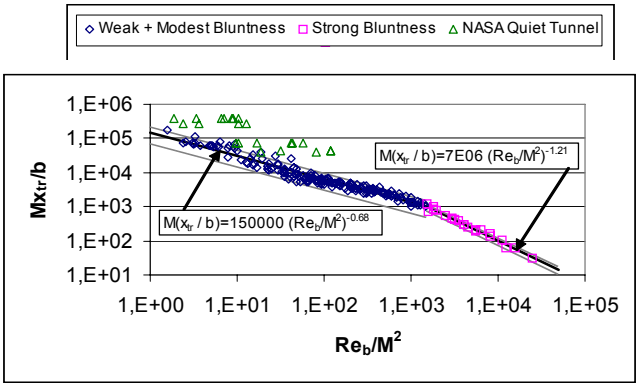


Fig. 2 Flat plate transition data correlation, including viscous - dominated data [3]

The combined "noisy" weak (viscous dominated) and modest bluntness data of Fig. 2, for $Re_b/M^2 < 1000$, correlates best (at +/- 50%) according to:

$$Re_{xtrans} = 150000 M^{0.36} Re_b^{0.32} \qquad (4)$$

while the NASA quiet tunnel data exhibits significantly enhanced stability when the tunnel is operated in the fully "quiet mode".

## 3 Cone Data Analysis

### 3.1 Data Sources

The cone transition data has been assembled in [19] from the work of [13-18]. Data covers a range in free-stream-based leading edge bluntness Reynolds number, $Re_b$, between 360 and 2.7 million and in free-stream-based transition onset Reynolds number, $Re_{xtrans}$, between 1.9 million and 44 million, for Mach numbers between 3.5 and 20. A brief outline of the data sets considered herein is given below.

#### *3.1.1 Mach 3.5 (NASA quiet tunnel) data*

The Mach 3.5 data has been collected in the NASA quiet tunnel [13] at the same tunnel operating conditions as the corresponding flat plate data of Fig. 2. A 5° half-angle cone with a 25μm nose diameter has been used at zero angle of attack in the experiments of [13] which were conducted at various degrees of "tunnel quietness", primarily associated with tunnel nozzle boundary layer bleeding. Cone transition data was taken at free-stream unit Reynolds numbers between 10 and 80 million per meter.

### *3.1.2 Mach 5 data*

The Mach 5 data [15] has been collected in the DLR Goettingen Ludwieg tube over a 5° half-angle cone model with nose diameters of 1.4, 3.5, 7, 10.5 and 17.5 mm. The free-stream unit Reynolds number was maintained at 24 million per meter.

Moreover, angle of attack was varied during these experiments in the range -3° thru +3°. Figure 3 shows the very interesting trends of transition Reynolds number as a function of nose bluntness and angle of attack [15].

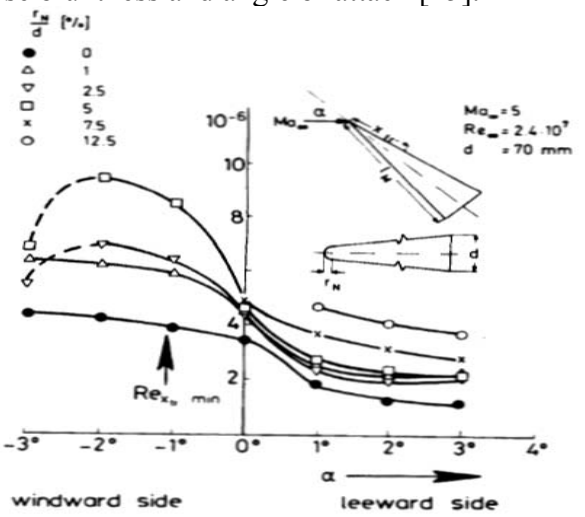


Fig. 3 Angle of attack effect on cone transition Reynolds number [15]

### *3.1.3 Mach 6 data*

The Mach 6 data [16] was collected at NASA's Langley Research Center, again using a 5° half-angle cone model with 50.8μm, 1.59mm and 3.18mm nose diameters at zero angle of attack. Free-stream unit Reynolds number varied between 7 and 26 million per meter.

### *3.1.4 Mach 8 data*

The Mach 8 data [14] was collected at AEDC tunnel B over a 7° half-angle cone with nose diameter of 102μm. Unit Reynolds number ranged between 40 and 120 million per meter.

### *3.1.5 Mach 9 data*

The Mach 9 data [17] has been collected at the No. 2 Gun Tunnel of Imperial College over a 5° half-angle cone with nose diameters of 2, 3, 3.5, 4, 6 and 50.8 mm. All tests were conducted at nominally zero incidence, with free-stream unit Reynolds numbers of 15 (at Mach 8.85) and 55 million per meter (at Mach 9.16).

It is interesting to note that the measured pressure distributions in this set of experiments (Fig. 4) indicate an initial overexpansion at approximately 25 nose radii followed by a recompression to the sharp cone pressure level downstream. Such overexpansion in the cone frustrum area is also picked up in the computations of [20], while the subsequent adverse pressure gradient is thought to have a destabilizing effect on frustrum transition [21].

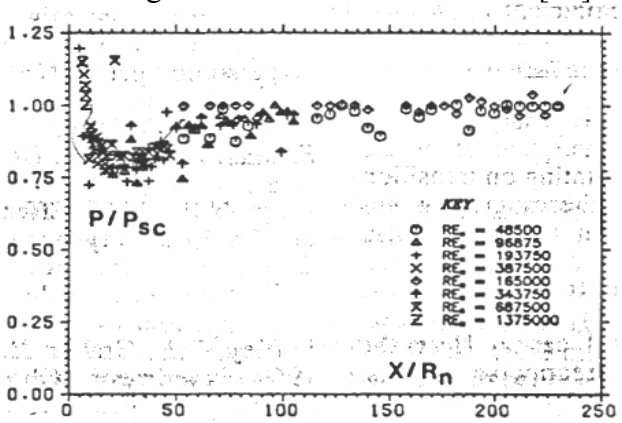


Fig. 4 Flow overexpansion around cone frustrum [17]

### *3.1.6 Mach 20 flight test data*

The Mach 20 data has been obtained [18] during a flight experiment using a 5° half-angle cone with an initial nose diameter of 5.08 mm, which ablated during the flight experiment to increasing values of nose bluntness. The nose bluntness variation during the flight test was estimated theoretically in [18] by three different methods (Fig. 5). Data was eventually reduced assuming the minimum and maximum nose ablation profiles of Fig. 5 (curves 1 and 3).

Measurements were taken during descent from 100,000ft to 60,000ft with the free-stream unit Reynolds number varying between 6.5 and 52.5 million per meter. In fact, results in [18] are presented on the basis of local (boundary layer edge) conditions, estimated from a blunt-nose equilibrium air model coupled with a boundary layer solution with variable entropy effects and assuming zero angle of attack. The approach of [18] yields a peculiar drop in local Mach number at an altitude of approximately 80,000 ft, which does not match a corresponding change in free-stream Mach number; this issue is further examined in section 3.2.7 below.

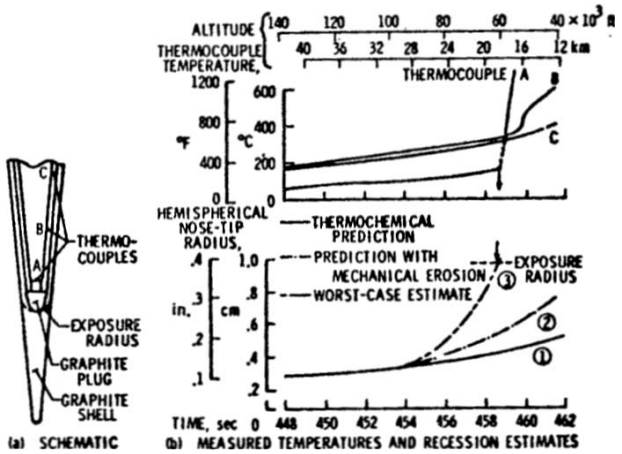


Fig. 5 Nose ablation models and evolution of nose bluntness [18]

It is also estimated in [18] that angle of attack during the flight test was less than 1°, still leading to a significant asymmetry of transition (onset and end) around the cone (Fig. 6).

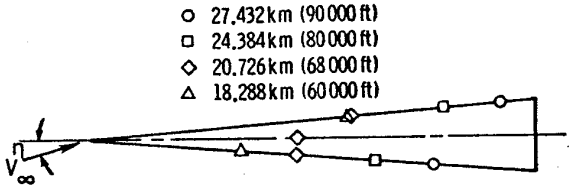


Fig. 6 End of transition asymmetry around cone due to small angle of attack [18]

It is seen in Fig. 6 that the windward side of the cone is more prone to transition than the leeward side. This result is noted in [18] to be "*contrary to most of the wind tunnel transition data at angle of attack, which shows that transition moves farther forward on the leeward side*", as is indeed the case with the data of [15] in Fig. 3 above. It is noted, however, that the trend of Fig. 6 (transition moving forward on the windward (rather than the leeward) side of the cone has been observed in other investigations too [22-24].

## 3.2 Data Processing and Evaluation

### *3.2.1 Estimation of local flow conditions*

For the purposes of data evaluation and correlation, a methodology for the estimation of local (boundary layer edge) flow conditions was required. Noting the variance in available information between the different data sources, it was decided to incorporate in the estimates of local flow conditions only the far-field effects of cone half-angle and angle of attack, if present. Consequently, free-stream conditions are transformed to local flow conditions by utilization of the (perfect gas) conical shock wave relations of [25], and neglecting any nose bluntness and viscous interaction effects.

This transformation proved to have only a small effect on the majority of the data, because of the small cone half-angles and angles of attack; the most pronounced effects (relative to using free-stream conditions) were expectedly found at the higher Mach number cases.

### *3.2.2 Mach 3.5 (NASA quiet tunnel) data*

The important effect of tunnel quietness on transition, previously shown for the flat plate case in Fig. 2, is found again in the cone data of [13]. Figure 7 shows, in the correlation form of Figs. 1 and 2, a comparison of the flat plate and cone data of [13] and the stabilizing effect of increasing tunnel quietness. It is noted that the cone data also falls at the low end of the $Re_b/M^2$ parameter, thus it is likely to be influenced by viscous effects, as is the flat plate data of [13]. Notably, flat plate and cone data, at the same level of tunnel quietness, are found to correlate well with each other.

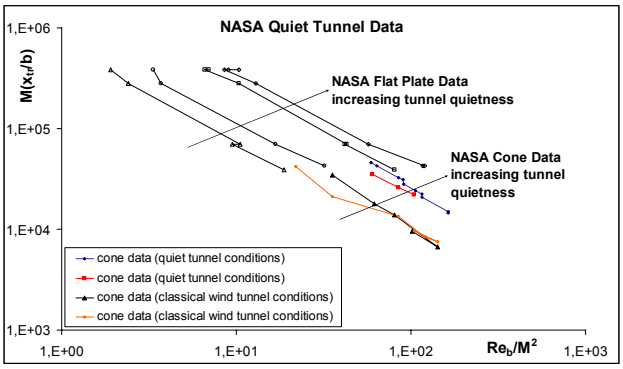


Fig. 7 Mach 3.5 flat plate and cone data from the NASA quiet tunnel in the proposed correlation form (local flow conditions)

### *3.2.3 Mach 5 data*

The Mach 5 data of [15] provide a systematic study of the influence of angle of attack on transition. The results of Fig. 3 are re-plotted in Fig. 8 in the form used for the present correlation purposes after [3].

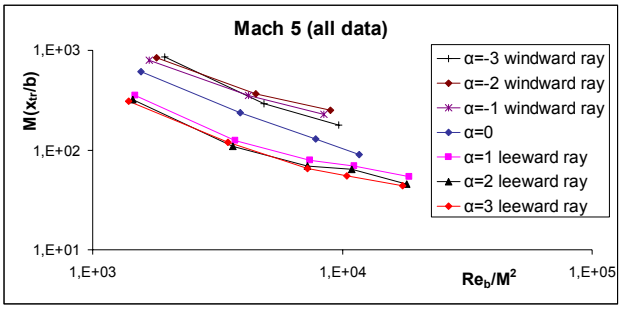


Fig. 8 Mach 5 cone data from the DLR Ludwieg tube in the proposed correlation form – effect of angle of attack (local flow conditions)

It is interesting to note in Fig. 8 that even a 1° angle of attack has an important stabilizing effect on the windward ray of the cone and an equally important destabilizing effect on the leeward ray. Further increases of the angle of attack up to 3° do not affect seriously the transition behaviour on either the windward or the leeward side of the cone. Moreover, the preceding discussion in section 3.1.6 is recalled, where the opposite angle of attack effects were found in the flight test data of 18].

### *3.2.4 Mach 6 data*

The Mach 6 data of [16] is plotted in Fig. 9 based on both free-stream and local flow conditions. Evidently, at such Mach number with only 5° cone half-angle, the change of free-stream flow conditions to local conditions over the cone surface (at zero angle of attack) has a rather small effect.

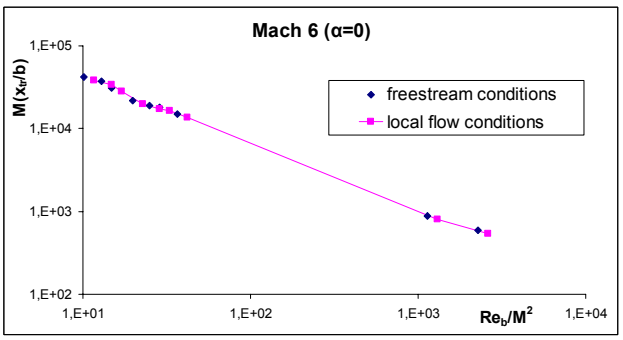


Fig. 9 Mach 6 cone data from NASA in the proposed correlation form – free-stream versus local flow conditions

### *3.2.5 Mach 8 data*

The Mach 8 data of [14] is similarly plotted in Fig. 10 based on both free-stream and local flow conditions. In this case of higher free-stream Mach number and larger cone half-angle of 7°, the change from free-stream to local flow conditions becomes evident.

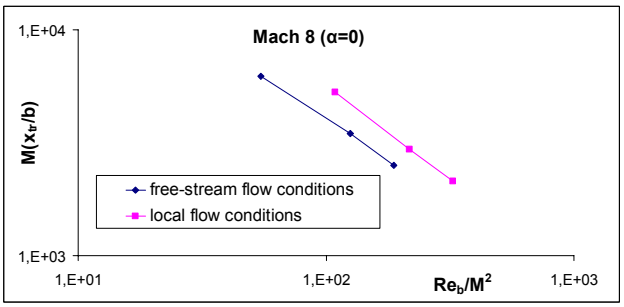


Fig. 10 Mach 8 cone data from AEDC in the proposed correlation form – free-stream versus local flow conditions

### *3.2.6 Mach 9 data*

The Mach 9 data of [17], shown in the proposed correlation format in Fig. 11, reduced at both free-stream and local flow conditions, exhibits a rather mild trend with increasing nose-bluntness Reynolds number, except for the highest Reynolds number and nose bluntness data point (the only measurement available for the 50.8 mm nose diameter model), where a significant forward movement of the transition location is observed. This trend variation could be due to possible modest (and random) differences from the nominal zero angle of attack assumed in the experiments.

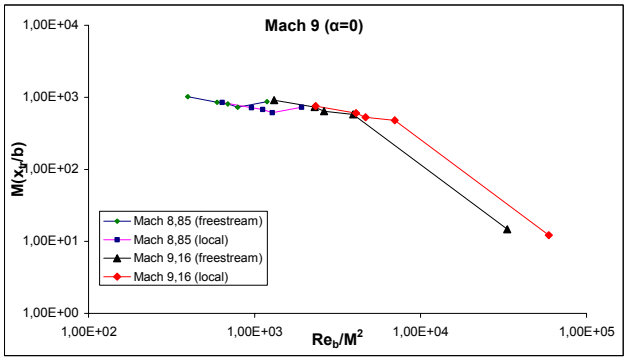


Fig. 11 Mach 9 cone data from Imperial College Gun Tunnel in the proposed correlation form – free-stream versus local flow conditions

### *3.2.7 Mach 20 flight test data*

The Mach 20 data, based on the local flow conditions provided in [18], is plotted in Fig. 12 for the two extreme nose bluntness evolution scenarios of Fig. 5.

Further to the discussion in section 3.1.6 and a detailed examination of the data provided in [18], the cause for the peculiar data trend of Fig.

12 has been traced to a sudden change in the local flow conditions estimated in [18], which occurs at an altitude of about 80,000 ft (Figs. 13 and 14), and not to any sudden forward movement of the transition onset location (Fig. 15). It is also seen in Figs. 13 and 14 that the free-stream Mach and unit Reynolds numbers (estimated directly from data provided in [18]) do not exhibit any sudden change that could correspond to the behaviour of the local flow conditions estimated in [18]. In contrast, when local flow conditions are calculated by the simple methodology of section 3.2.1, the trend in Figs. 13 and 14 remains similar to the trend of the raw free-stream conditions (and different from the local flow condition estimate of [18]).

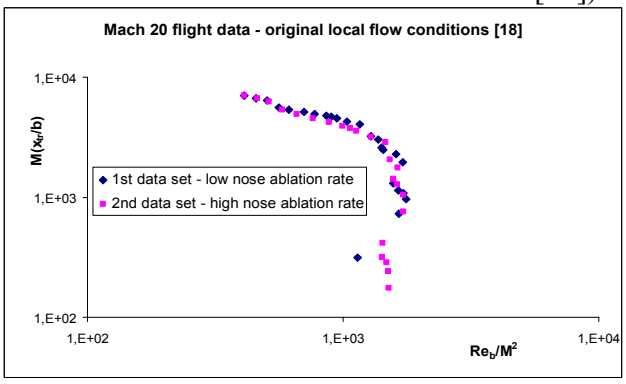


Fig. 12 Mach 20 flight test cone data in the proposed correlation form –local flow conditions with two extreme nose bluntness variation profiles

Notwithstanding the fact that the present estimates of local flow conditions agree with the estimates of [18] at high altitudes (despite the inviscid perfect gas flow assumed in the methodology of section 3.2.1), it is likely that the discrepancy stems from the treatment in [18] of boundary layer growth (and viscous interaction) at altitudes below 80,000 ft.

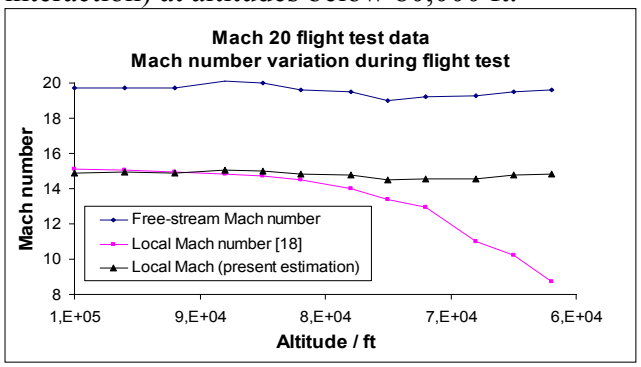


Fig. 13 Mach 20 cone flight test – free-stream versus local Mach number

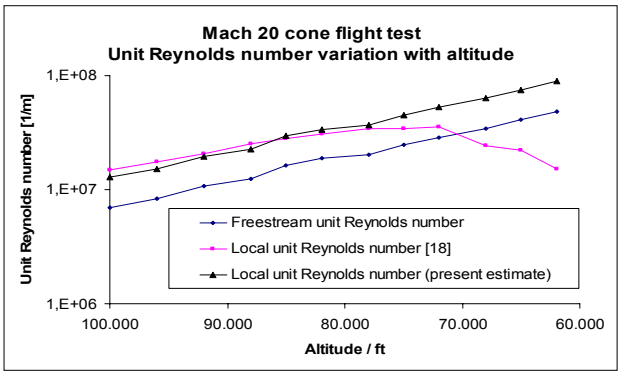


Fig. 14 Mach 20 cone flight test – free-stream versus local unit Reynolds number

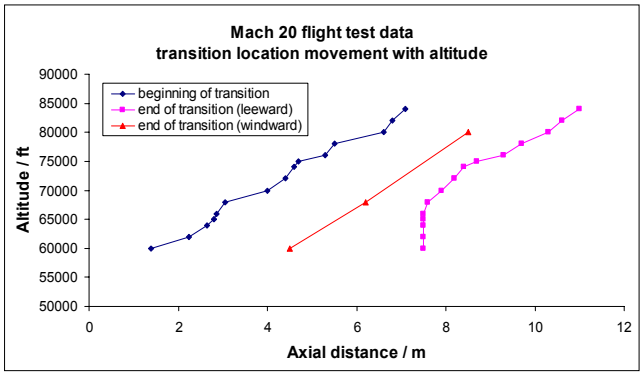


Fig. 15 Mach 20 cone flight test – transition location versus flight altitude

In view of the above, the Mach 20 flight test data is processed in Fig. 16 (assuming in this case the strong nose ablation profile of Fig. 5) according to the free-stream flow conditions given in [18] and the local flow conditions estimated as per section 3.2.1 above.

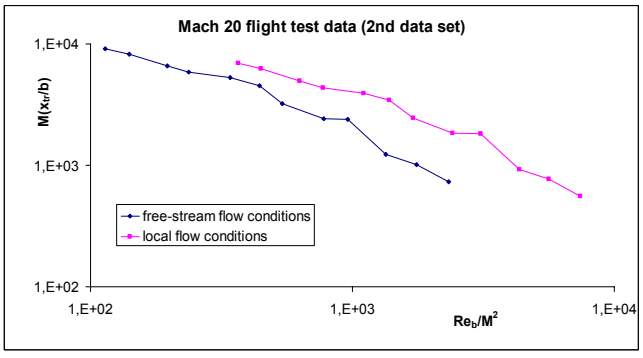


Fig. 16 Mach 20 flight test cone data in the proposed correlation form – free-stream vs. local (as per section 3.2.1) flow conditions, assuming the strong ablation nose bluntness variation profile

Lastly, with reference to the discussion in section 3.1.6, it is recalled that the data of Fig. 16 corresponds to the leeward ray of the cone with a typical angle of attack of order 1°.

### 3.3 Cone Data Correlation

For the present correlation purposes, local flow conditions are used to accommodate the effects of cone half-angle (and, when applicable, angle of attack) on Mach and Reynolds numbers. The entirety of the cone data examined herein is plotted in the proposed correlation form in Fig. 17, based on local flow conditions. According to the preceding discussion, this data includes the significant effects of (small) angle of attack on transition onset location (which have been found to be insensitive to the absolute value of the angle of attack), while they are likely to be related to the presence of cross-flow over the conical body at incidence.

Indicatively, also shown in Fig. 17 is the correlation of the zero angle of attack cone data, eq. (6), established herebelow in Fig. 18, with a +/- 50% band around it. The scatter observed in the data of Fig. 17 is well in excess of this +/- 50% band and, thus, prohibitive for correlation purposes. Evidently, the greatest divergence (enhanced stability) in Fig. 17 is found for the NASA quiet flow data, the Mach 20 flight test data on the leeward side of the cone at $1^{o}$ angle of attack, and some of the Mach 9.16 data, which is probably affected by varying angle of attack in the experiments. At the lower Mach number of 5, the shift of transition onset location due to angle of attack is not as pronounced.

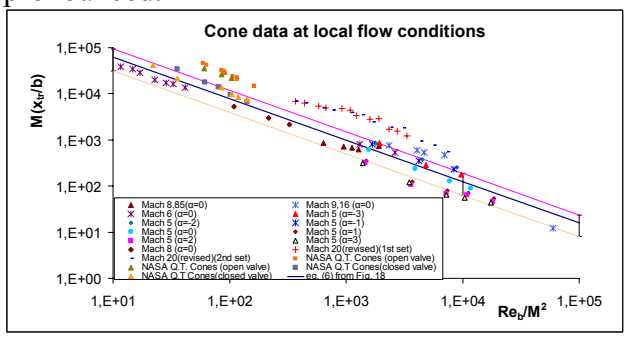


Fig. 17 Cone data in the proposed correlation form – local flow conditions

If now, the known zero angle of attack data is isolated and plotted in Fig. 18, a number of observations can be made. Regarding the Mach 5, 6 and 8 measurements at zero incidence, these may be correlated by a single curve, despite the fact that they extend over both of the previously identified flat plate regimes, namely the modest and the strong bluntness regimes [3]. The single cone transition onset correlation curve then reduces to the form:

$$\mathrm{Re}_{xtrans} = 320000 M^{0.72} \mathrm{Re}_b^{0.14} \qquad (5)$$

or, if the "poor quietness" data of [13] is also included, to the form:

$$\mathrm{Re}_{xtrans} = 500000 M^{0.80} \mathrm{Re}_b^{0.10} \qquad (6)$$

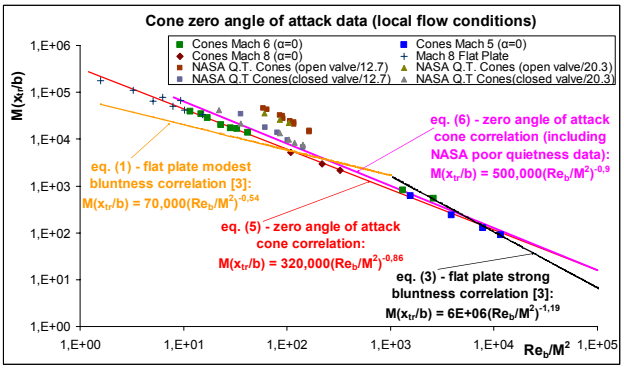


Fig. 18 Zero angle of attack cone data in the proposed correlation form – local flow conditions

Shown for comparison in Fig. 18 are the correlation curves of [3] for modest and strong bluntness flat plate transition (Fig. 1; eqs. (1) and (3)). The trend of the cone data is generally similar to the flat plate correlation curves, particularly in the strong bluntness flat plate regime; in the modest bluntness regime, the cone data exhibits a more stable behavior than eq. (1). It is also interesting to recall from Fig. 7 that the NASA quiet tunnel flat plate data (which has exhibited a more stable behavior than the bulk of the weak / modest bluntness data in [3]), correlates well with cone data at the same level of tunnel quietness. Similarly, the Mach 8 AEDC flat plate data is seen in Fig. 18 to follow eq. (5) or (6) more closely than eq. (1).

## 4 Complete Vehicle Transition Data

### 4.1 Space Shuttle Orbiter Flight Tests

Significant flight test data has been accumulated and documented in [26] from the extensive Orbiter Flight Test (OFT) program, applied to the first four Space Transportation System

flights (STS 1-4), as well as from STS 5 (which was the first operational flight of the Space Shuttle). Amongst this data, transition location along the windward symmetry line of the vehicle has been monitored during re-entry at free-stream Mach numbers between 13.5 and 0.7, and the data is presented and analyzed in [27].

The raw data, in the form of transition onset location versus time during re-entry, is presented in Fig. 19. It is seen that, for each flight, transition is first detected at the rearmost part of the windward symmetry line of the Shuttle and, in a transient, almost instantaneous manner, shifts rapidly forward to approximately 0.2 of the reference Shuttle length. Thereafter, the transition location continues to move smoothly forward as the vehicle descends towards the earth's surface.

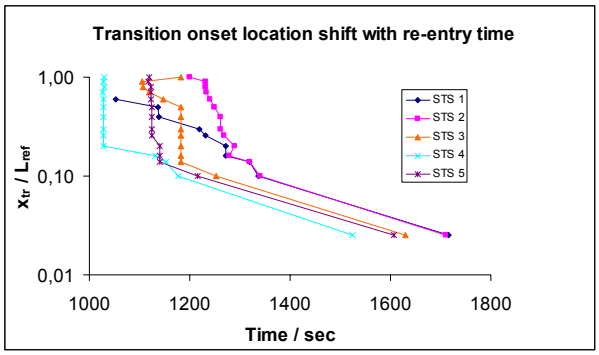


Fig. 19 Space Shuttle Orbiter raw transition data

For the purposes of this paper, where (quasi-) steady-state, supersonic flow transition is examined, the data representing the initial transient movement of the transition onset location is excluded. Moreover, it is noted that the most forward transition location measured during each of STS 1-5 [27] (effectively on the nose cap of the Shuttle, at 0.025 of the vehicle reference length), corresponds to subsonic flow (at a small angle of attack of $5^o$-$7^o$ during the final stages of descent) and is, thus, also excluded from this presentation.

Consequently, the limited Space Shuttle transition data that qualifies for consideration herein covers a range in free-stream Mach number between 10 and 5; in terms of local flow conditions, provided in [27], the Mach number remains almost constant at a value of about 2, and the unit Reynolds number varies between 0.1 and 0.6 million per meter. Angle of attack in this part of descent varied between $25^o$ and $40^o$.

Of particular concern for the purposes of this paper is also the "effective" nose bluntness that applies to the (full scale) Space Shuttle configuration. In fact, following the approach of representing the (windward symmetry line of the) Space Shuttle by an axisymmetric analogue configuration [28], the "effective" nose bluntness of the Orbiter can be well approximated by a linear variation of nose diameter, from 0.986 m at $21.8^o$ angle of attack to 2.736 m at $42.75^o$, i.e. by:

$$b = 0.0835(\alpha - 10) \text{ for } 21.8^o<\alpha<42.75^o \qquad (7)$$

Figure 20 shows the Orbiter symmetry line transition data, selected and processed in accordance with the preceding discussion, and reduced to the proposed correlation form using local flow conditions from [27] and eq. (7) for the nose bluntness. Also shown is the more extensive set of measurements presented in [27] with free-stream flow conditions, assuming this time a constant "effective" nose bluntness of 1m (rather than the variation of eq. (7)). For comparison, the data is also presented using local flow conditions and a constant "effective" nose diameter of 1m.

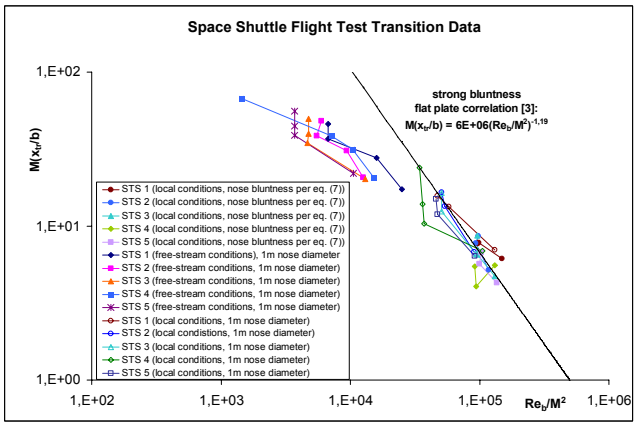


Fig. 20 Space Shuttle Orbiter (STS 1-5) transition data in the proposed correlation form

The strong bluntness flat plate correlation curve of [3], as it applies to this range of $Re_b/M^2$, is illustrated in Fig. 20 to provide a very good approximation to the selected Shuttle windward symmetry line transition data, when treated with local flow conditions, independent of which nose bluntness model is incorporated.

## 4.2 X-33 and X-34 Ground Test Results

A 0.0132-scale model of the blunted slab - delta planform X-33 vehicle has been tested at Mach 6 in the NASA LaRC 20-inch wind tunnel at $20^o$, $30^o$ and $40^o$ angle of attack, with free-stream unit Reynolds numbers of 13 and 27 million per meter [29, 30]. The nose diameter in the experiments was 32 mm, and has been utilized for the present data processing independent of angle of attack. Similar experiments were conducted in the same facility also on the slender X-34 vehicle configuration at $15^o$ angle of attack [31, 32]. The nose diameter of this vehicle was 6.65 mm.

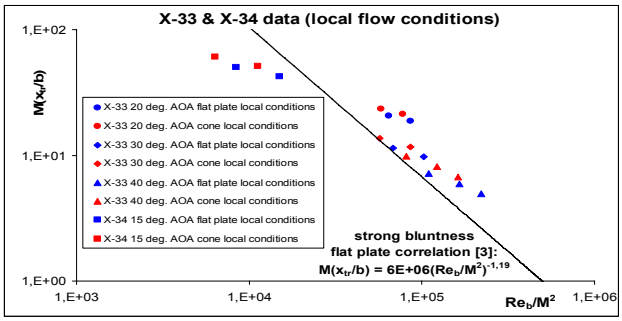


Fig. 21 X-33 & X-34 transition data in the proposed correlation form (local flow conditions)

In both cases, local (windward symmetry line) flow conditions have been estimated assuming a perfect gas flat plate at incidence, as well as a zero angle of attack cone with the corresponding half-angle. Figure 21 shows the X-33 and X-34 transition data at such local flow conditions, and a comparison with the flat plate strong bluntness correlation, eq. (3). The X-33 data is in reasonable agreement with the correlation, with the exception of the $20^o$ angle of attack data where transition has been measured at the rear of the model [30] and may have been influenced by the base of the configuration; hence, the $20^o$ angle of attack X-33 data is excluded from further processing. The X-34 data on the other hand shows a less stable behaviour than the proposed correlation.

## 5 Summary and Conclusion

The entirety of the transition onset data considered herein is summarized (at local flow conditions) in Fig. 22. It is found that the strong bluntness correlation, eq. (3), or its similar form shown in Fig. 22, represent not only the data for $Re_b/M^2>1000$, but a general upper bound for transition onset throughout the data range. At $Re_b/M^2<1000$, the majority of the data exhibits reduced stability, and an important influence of flow disturbance parameters; in this data range, the lower transition bound is closely represented by the flat plate modest bluntness correlation, eq. (1).

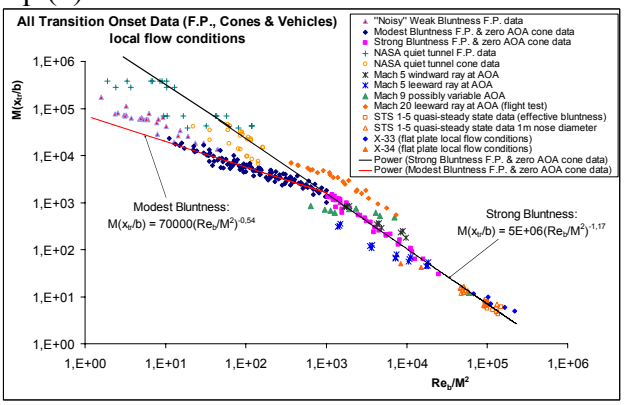


Fig. 22 Complete set of transition onset data in the proposed correlation form (local flow conditions)

Note is finally made to the puzzling effects of (small) angle of attack on transition over slender (conical) configurations, manifested for example by the contradicting observations on the leeward side of the Mach 5 cone experiments (destabilizing) and the Mach 20 flight test (stabilizing) and, to a lesser extent, on the windward side of the Mach 5 cones and the X-34 vehicle, which deserve further attention.

## References

[1] Simeonides G. Leading edge bluntness effects on flat plate boundary layer transition – compilation of high speed experimental data. ESA-ESTEC *Doc. YPA/1881/GS*, 1996.

[2] Simeonides G. Correlation of laminar-turbulent transition data over flat plates in supersonic / hypersonic flow including leading edge bluntness effects. *Shock Waves*,Vol.12,No.6, pp.497-508, 2003.

[3] Simeonides G. Laminar-turbulent transition correlations in supersonic / hypersonic flat plate flow. *24th ICAS Congress*, Yokohama, Japan, 2004.

[4] Heffner K. and Arnal D. Leading edge bluntness effect on laminar-turbulent boundary layer transition on a flat plate at Mach 7. CERT-ONERA *RT-93/5618.98*, 1994.

[5] Cazenave F. Etude numerique des effets de l'emoussement de plaques planes sur la transition en

ecoulement supersonique et hypersonique. Ph.D. Thesis, ENSAE, 1993.

[6] Simeonides G. Hypersonic shock wave boundary layer interactions over compression corners. Ph.D. Thesis, von Karman Institute / Univ. Bristol, 1992.

[7] Boerrigter H.L., Charbonnier J.M. and Elbay M.K. Quantitative boundary layer transition measurements on flat plates and cones in hypersonic flow. *EUROMECH 312*, VON Karman Institute Preprint 1994-05, 1993.

[8] Boerrigter H.L. and Charbonnier J.M. On the effect of flowfield non-uniformities on boundary layer transition in hypersonic flow. *EUROMECH 330*, von Karman Institute Preprint 1995-19, 1995.

[9] Maslov A.A. et al. Hypersonic boundary layer stability and transition. ITAM Report (communicated by Aerospatiale Espace et Defense to ESA/ESTEC in the frame of the 1994-1996 ESA TRP program on transition), 1994.

[10] Potter J.L. and Whitfield J.D. Effects of unit Reynolds number, nose bluntness and roughness on boundary layer transition. *AEDC-TR-60-5*, 1960.

[11] Pate S.R. and Groth E.E. Boundary layer transition measurements on swept wings with supersonic leading edges. *AIAA Journal*, Vol. 4, No. 4, pp. 737-738, 1996.

[12] Jillie D.W. and Hopkins E.J. Effects of Mach number, leading edge bluntness and sweep on boundary layer transition on a flat plate. *NASA TN D-1071*, 1961.

[13] Chen F.J., Malik M.R. and Beckwith I.E. Boundary layer transition on a cone and flat plate at Mach 3.5. *AIAA Journal*, Vol. 27, No. 6, pp. 687-693, 1989.

[14] Stetson K.F., Kimmel R.L., Thompson E.R., Donaldson J.C. and Siler L.G. A comparison of planar and conical boundary layer stability and transition at a Mach number of 8. *AIAA 22nd Fluid Dynamics, Plasma Dynamics and Lasers Conference*, Honolulu, AIAA Paper 91-1639, 1991.

[15] Schoeler H., Banerji A. Visualization of boundary layer transition on a cone with liquid crystals, *ICIASF'83 Record of International Congress on Instrumentation in Aerospace Simulation Facilities*, 1983.

[16] Horvath T.J., Berry S.A., Hollis B.R., Chang C.L., Singer B.A. Boundary layer transition on Slender Cones in Conventional and Low Disturbance Mach 6 Wind Tunnels", *32nd AIAA Fluid Dynamics Conference and Exhibit*, St. Louis, Missouri, 2002.

[17] Sell M., Hillier R. Transition Studies on Blunted Cones at Hypersonic Speed. Imperial College of Science, Technology and Medicine, Department of Aeronautics, London, UK.

[18] Wright R.L., Zoby E.V. Flight Boundary Layer Transition Measurements on a Slender Cone at Mach 20, *AIAA 10th Fluid & Plasma Dynamics Conference*, Albuquerque, New Mexico. 1987.

[19] Kosmatopoulos E. Correlation of supersonic flow laminar-turbulent transition data, Diploma Thesis, Laboratory of Mechanics of Fluids and Applications, Dept. Mechanical and Aeronautical Engineering, Univ. Patras, 2005.

[20] Malik M.R., Spall R.E. and Chang C-L. Effect of nose bluntness on boundary layer stability and transition. *AIAA Paper 90-0112, 28th Aerospace Sciences Meeting*, Reno, 1990.

[21] Stetson K.F. Hypersonic boundary layer transition. *3rd Joint Europe / U.S. Short Course in Hypersonics*, Univ. Aachen, 1990.

[22] Martelucci A. and Neff R.S. The influence of asymmetric transition on reentry vehicle motion. *AIAA Paper 70-987*, 1970.

[23] Madalon D.V. and Henderson A. Jr. Hypersonic transition studies on a slender cone at small angles of attack. *AIAA Journal, Vol. 6, No. 1*, Jan. 1968, pp. 176-177.

[24] Bushnell D.M., Jones R.A. and Huffman J.K. Heat transfer and pressure distributions on spherically blunted 25° half-angle cone at Mach 8 and angles of attack up to 90°. *NASA TN D-4792*, 1968.

[25] Ames Research Staff. Equations, tables and charts for compressible flow. NACA Report 1135, 1953.

[26] Shuttle Performance: Lessons Learned. *NASA Conference Publication 2283*, March 1983.

[27] Goodrich W.D., Derry S.M. and Bertin J.J., Shuttle Orbiter Boundary Layer Transition: a Comparison of Flight and Wind Tunnel Data. *AIAA Paper, No 83–0485, 21st Aerospace Sciences Meeting,* Jan. 1983 (also included in Part II of [26], pp. 753-779).

[28] Hamilton H.H., DeJarnette F.R. and Weilmuenster K.J. Application of Axisymmetric Analog for Calculating Heating in Three-Dimensional Flows. *AIAA J. Spacecraft,* Vol. 24, No. 4, 1987.

[29] Horvath T.J., Berry S.A., Hollis B.R., Liechty D.S., Hamilton II H.H. and Merski N.R.. X-33 Experimental Aeroheating at Mach 6 Using Phosphor Thermography. *AIAA Paper 99-3558, 33rd Thermophysics Conference*, Norfolk VA, July 1999.

[30] Berry S.A., Horvath T.J., Hollis B.R., Thompson R.A. and Hamilton II H.H. X-33 Hypersonic Boundary Layer Transition. *AIAA Paper 99-3560, 33rd Thermophysics Conference*, Norfolk, July 1999.

[31] Berry S.A., Horvath T.J., DiFulvio M., Glass C. and Merski N.R. X-34 Experimental Aero-heating at Mach 6 and 10. *AIAA Paper 98-0881, 36th AIAA Aerospace Sciences Meeting & Exhibit*, Jan. 1998.

[32] Merski N.R. Reduction and Analysis of Phosphor Thermography Data with the IHEAT Software Package. AIAA Paper 98-0712, 36th AIAA Aerospace Sciences Meeting and Exhibit, Reno, January 1998.